Investigations into the drying kinetics of biomass in a fluidized bed dryer using electrostatic sensing and digital imaging techniques

Yong Yan[1,2], Bojian Qi[1,*], Wenbiao Zhang[1], Xueyao Wang[1], Qingqing Mo[1]

1. School of Control and Computer Engineering, North China Electric Power University, Beijing 102206, China
2. School of Engineering, University of Kent, Canterbury, Kent CT2 7NT, UK

(* Corresponding author: bojianqi@ncepu.edu.cn)

Abstract

Investigations into drying kinetics of biomass in fluidized bed dryers are essential for the control of drying processes, enhancing productivity and reducing energy consumption. However, there is limited research on drying characteristics of biomass at different bubble locations due to complex hydrodynamics around bubbles in the bed. In this paper, a new method is proposed by combining electrostatic sensing and digital imaging techniques to obtain moisture contents, drying models, moisture diffusivities, activation energies and mass transfer coefficients of biomass at different bubble locations. Experimental tests were conducted on a laboratory-scale fluidized bed dryer for different air velocities at a range of air temperatures. Five mathematical drying models are evaluated in the paper. It is found that the Page drying model is most suitable for describing the drying process of biomass in the fluidized bed. The results also show that the mass transfer coefficient of biomass at the interior and boundary of the bubble is higher than that at the exterior of the bubble. In addition, although the mass transfer coefficient increases with the air temperature and air velocity, the highest air temperature and highest air velocity are not optimal conditions. For example, a bubble flow turns into a slug flow or plug flow at an air velocity of 0.56 m/s and an air temperature of 75 ℃.

Keywords: *Fluidized bed dryer; biomass; drying kinetics; electrostatic sensing; digital imaging*

Nomenclature

Symbols

a	Fitted coefficient in Eqs. (8) − (9)
A_p	Surface area of biomass, m^2

34	c	Fitted coefficient in Eq. (9)
35	D_{eff}	Moisture diffusivity, m^2/s
36	D_0	Moisture diffusivity at infinite moisture content, m^2/s
37	E_a	Activation energy, kJ/mol
38	k	Fitted coefficient in Eqs. (5) − (9)
39	k_{gp}	Mass transfer coefficient between biomass and air, m/s
40	M	Moisture content, wt. %
41	M_e	Equilibrium moisture content, wt. %
42	M_0	Initial moisture content, wt. %
43	M_t	Moisture content at drying time t, wt. %
44	$\dot{m}_v$	Water vapour mass flow rate transferred between biomass and air, kg/s
45	N	Number of data points
46	n	Fitted coefficient in Eqs. (6) − (7)
47	P	Number of parameters in a fitting function
48	R^2	Coefficient of determination
49	r	Biomass radius, m
50	RH	Relative humidity of drying air, %
51	S	Summed square of residuals
52	S_p	Surface area per unit volume of solids, m^2/m^3
53	T	Temperature, K
54	t	Time, s
55	V_p	Biomass volume, m^3
56	w_d	Biomass weight after drying, kg
57	w_t	Biomass weight before drying, kg
58		
59	*Greek letters*	
60	$\alpha_{v,i}$	Mass concentration of moisture in air at bed entrance, kg/m^3
61	$\alpha_{v,o}$	Mass concentration of moisture in air at bed exit, kg/m^3

$\alpha_{v,s}$ Mass concentration of moisture in air on particle surface, kg/m^3

$\Delta\alpha_{ml}$ Logarithmic mean difference in mass concentration of moisture in air, kg/m^3

η Drying rate, wt. %/s

$\rho_{p,0}$ Density of dry biomass, kg/m^3

ϕ Moisture ratio

χ^2 Reduced Chi square

1. Introduction

In order to reduce greenhouse gas emissions, biomass fuels are used as substitutes for fossil fuels in the energy and energy-intensive industries [1-3]. Many biomass fuels are produced from raw agricultural materials often with high moisture content. The moisture content in biomass fuels decreases their heating value, hence they should be dried before combustion [4]. Moreover, drying is beneficial for some industrial processes, for instance, drying corns is an important procedure before bioethanol production [5]. However, the drying process consumes a significant amount of energy [6, 7]. Various methods are used for drying of biomass. In view of the advantage of good heat and mass transfer rates and efficient particle mixing inside reactors, fluidized beds are widely used for biomass drying [8]. Fluidized bed drying is a complex and chaotic process involving simultaneous heat and mass transfers in a transient state, which depend on various factors such as biomass structure, physicochemical properties, and operating conditions (i.e. velocity, temperature and humidity of the drying medium) [9]. Furthermore, bubbles in a gas-solid fluidized bed increase complexities of the drying kinetics as particles at different locations such as interior, boundary and exterior of the bubble have different contact phenomena with the hot air [10]. In order to predict drying behaviors, control and optimize a fluidized bed dryer, and maintain biomass fuels with the desired moisture content, a profound knowledge of biomass drying kinetics in the fluidized bed is essential.

The drying of biomass in a fluidized bed has been widely reported in the literature. Biomass drying kinetics such as moisture content, drying model, moisture diffusivity, activation energy, and mass transfer coefficient between biomass and air have been studied [11, 12]. There are many techniques available for measuring the moisture content of solids in a fluidized bed dryer. These include near infrared spectroscopy, acoustic emission detection, electrical capacitance tomography (ECT) and microwave resonance as well as

triboelectric sensing with probes, as mentioned in a recent review paper [11]. Furthermore, a number of mathematical models for the drying process have been developed by investigating the drying behaviors and drying time of moist products. These models are also useful for the prediction of heat and mass transfer characteristics of a range of bulk solids. Therefore, it is necessary to evaluate and compare the drying models for a given biomass [12]. In the modelling of the drying process, thin layer drying equations have been widely applied [13, 14]. Chen *et al.* investigated the kinetic analysis of raw biomass through thermogravimetric analysis and a comparison between different drying models based on statistical analysis [13].

The moisture content in a moist biomass is reduced through diffusion within its body and evaporation from its surface. To evaluate the effect of moisture reduction through diffusion, moisture diffusivity was calculated [15, 16]. Jia *et al.* obtained effective diffusive coefficients of Douglas-fir sawdust using experimental data from drying tests in a pulsed fluidized bed. The moisture diffusivity was found to be in the range of 4.993×10^{-9} to 7.467×10^{-9} m^2/s under various pulsation frequencies and air flow rates [17]. The moisture diffusivity was then used to determine the activation energy of biomass, which characterizes the difficulty in overcoming energy barriers when water molecules migrate within particles [18]. Over the last few decades, convective mass transfer at the gas-solid interface has been studied to predict the mass transfer efficiency of fluidized bed drying [10, 19]. Moreno *et al.* [10] reported a method for the determination of the convective mass transfer coefficient for the drying of forest biomass particles in a fluidized bed, which ranged from 6×10^{-3} to 2×10^{-2} m/s. In addition, an equation that uses both Sherwood and the Reynolds numbers was proposed by Moreno *et al*. [10]. A non-invasive infrared technique was utilized in a fluidized bed to determine the gas-solid mass transfer coefficient and its correlations with the bubble size and superficial gas velocity by Medrano *et al.* [19]. However, such earlier research has focused on the macro characteristics of particles in a fluidized bed instead of identifying the discrepancies in the drying characteristics of particles at different locations of bubbles.

Recent studies [20, 21] reported the complexities of the drying process in a fluidized bed and challenges in quantifying the drying characteristics of biomass due to the presence of bubbles. The studies indicated that varied drying kinetics of biomass were presented at different locations (i.e. bubble interior, bubble boundary, and bubble exterior). The moisture content distribution of biomass particles in a fluidized bed was measured

using ECT methods [22, 23]. It was found that the moisture content of particles inside the void and bubble was low, while the moisture content of particles far from the bubble was high [22]. Moreover, electrostatic sensing techniques have also been proposed to measure the moisture content in biomass in a fluidized bed [24, 25]. In the electrostatic sensing method, an empirical model was established with the key parameters obtained by fitting the experimental data. Furthermore, the moisture content in biomass was inferred from the signals from a set of two-dimensional electrostatic sensor array. Qi *et al.* [21] studied the moisture content distribution of biomass particles in a fluidized bed dryer by combining electrostatic sensing and digital imaging techniques. It has been found that there are significant differences in the moisture content of biomass at the interior, boundary and exterior of the bubble in the bed [21]. Although the previous studies are useful, it is still necessary to conduct further in-depth analysis of the drying kinetics of biomass at different bubble locations. For instance, the mass transfer coefficient between biomass and air at different bubble locations is still unclear. Additionally, a fluidized bed dryer should be operated under optimized conditions to maintain high drying efficiency.

In a fluidized bed dryer, chaotic movement of fluid along with heat and mass transfers occurs, which brings a challenge for all existing methods to determine the optimal drying model, moisture diffusivity and mass transfer coefficient of biomass particles at different locations in a fluidized bed. The above parameters are difficult to predict analytically because they depend on the transport properties of the fluid, dynamic characteristics of the flow around particles, flow patterns and geometries of the bed [9]. Therefore, an appropriate method is desirable to determine the kinetic parameters of biomass and the optimal drying conditions. This paper aims to investigate the drying kinetics of biomass particles at different locations in a fluidized bed. Experimental tests were conducted on a lab-scale fluidized bed dryer with biomass corn kernels as test particles. The moisture content and bubble distributions are obtained by combining electrostatic sensing and digital imaging techniques. Finally, the drying characteristics of biomass at different locations in the fluidized bed are measured and discussed.

2. Methodology

2.1. Overall strategy

Fig. 1 shows the key stages in the proposed method. Firstly, an electrostatic sensor array and a digital camera are used to acquire electrostatic signals and images of biomass particles, respectively. Moisture content

distributions of biomass and bubble locations are derived, respectively. Secondly, images of the moisture content distribution marked with bubble locations (i.e. fusion images) are generated to extract useful information to determine the drying kinetics (i.e. moisture content curves, moisture diffusivities and gas-solid mass transfer coefficients). Subsequently, moisture content curves are used to derive the optimal drying model under given conditions. Meanwhile, moisture diffusivities are determined from the moisture contents. Activation energies of biomass are determined from the fitting curves of moisture diffusivities. Moreover, from the fusion images, the drying characteristics of biomass at different bubble locations are compared and the effects of the operation condition on the drying characteristics are explored. Important drying kinetics of biomass in the fluidized bed are finally obtained.

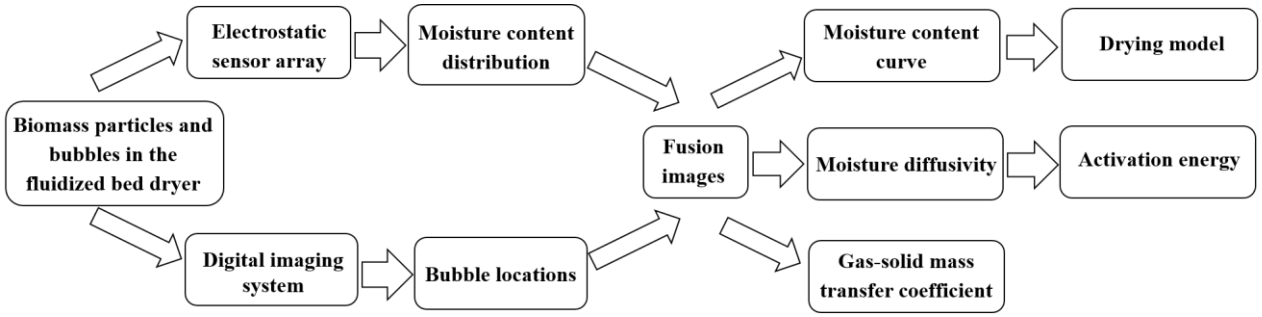

Fig. 1. Key stages in the proposed method.

2.2. Fusion image

In a fluidized bed, triboelectric charging is inevitable due to continuous particle-particle, particle-wall, and particle-air interactions [26]. The moisture content in biomass affects the charge due to the fact that water molecules as charge carriers dissipate the charge into free space and reduce the accumulation of the charge. It should be noted that, the water molecules migrate through diffusion within the pores of biomass and evaporation from the surfaces of biomass particles during drying process. The charge might be dissipated into the pores and the surfaces of biomass, which requires further studies in a molecular scale. Through electrostatic sensing the moisture content in biomass is measured from empirical relationships between the amplitude of the voltage signal from the electrostatic sensor array and the moisture content. As reported in an earlier study, an empirical model was established by fitting the experimental data [21]. Moreover, to validate the results from the electrostatic sensing method, biomass samples were taken from the fluidized bed and their moisture content was measured off-line with a Halogen Moisture Analyzer (Model HE83, Mettler Toledo). The experimental results demonstrated that the electrostatic sensor array is capable of measuring the moisture content with a relative error within ±15% [21]. The moisture content distribution in the fluidized bed is then reconstructed using a biharmonic spline interpolation (BSI) algorithm [27]. The drying kinetics parameters of biomass are then determined from a set of empirical equations (Section 2.3).

Real-time images of biomass in the fluidized bed dryer are obtained using the digital imaging system. The images are then processed using image processing algorithms to extract bubble locations. In addition, the bubble locations are marked on the images of the moisture content distribution to obtain fusion images. Finally, the drying characteristics of biomass at the interior, boundary and exterior of the bubble are determined from the values of the moisture content at corresponding pixels.

2.3. Drying kinetics

The moisture content in biomass is defined and determined from,

$$M = \frac{w_t - w_d}{w_d} \times 100\% \tag{1}$$

where w_t and w_d are biomass weights before and after drying, respectively.

The drying rate is expressed as,

$$\eta = \frac{M_{t_1} - M_{t_2}}{t_1 - t_2} \tag{2}$$

where η is the drying rate of biomass during the drying period from t_1 to t_2; M_{t_1} and M_{t_2} are the moisture contents in biomass at t_1 and t_2, respectively.

The moisture ratio of biomass (ϕ) is calculated from,

$$\phi = \frac{M_t - M_e}{M_0 - M_e} \tag{3}$$

where M_t and M_0 represent the current and the initial moisture contents in biomass, respectively. The following equation provides an equilibrium moisture content in biomass M_e [28],

$$M_e = \left(\frac{-\ln(1 - RH)}{8.654 \times 10^{-5} (T + 49.81)} \right)^{\frac{1}{1.8634}} \tag{4}$$

where RH is the relative humidity of the drying air and T is the ambient temperature.

Among all the existing models describing the drying kinetics of biomass, five typical models have been extensively used [13, 14]. Therefore, they are considered in this study. These models are as follows:

The Newton model,

$$\phi = \exp(-kt) \tag{5}$$

The Page model,

$$\phi = \exp(-kt^n) \tag{6}$$

198 The Modified Page model,

199 $$\phi = \exp\left[-(kt)^n\right] \tag{7}$$

200 The Henderson and Pabis model,

201 $$\phi = a\exp(-kt) \tag{8}$$

202 The Logarithmic model,

203 $$\phi = a\exp(-kt) + c \tag{9}$$

204 Where t is the drying time, k, n, a and c are model parameters in the above models.

205 These models are similar, as indicated by the similarity of the equations. In this study, these models are
206 compared with the experimental data before the optimal model for the drying process is then identified.
207 Furthermore, the parameters in the drying models are determined using the least-squares method, which
208 minimizes the summed square of the residuals between the measured and fitted moisture ratios, i.e.

209 $$S = \sum_{i=1}^{N}\left(\phi_{\exp,i} - \phi_{\mathrm{pre},i}\right)^2 \tag{10}$$

210 where S is the summed square of residuals, N is the number of data points, and $\phi_{exp,i}$ and $\phi_{pre,i}$ are the
211 measured and predicted moisture ratio, respectively. In order to investigate the moisture transfer during the
212 drying process, the moisture diffusivity, which is dependent on the moisture content and ambient
213 temperature, should be measured. The moisture diffusivity of biomass is described by the Fick's law [29]
214 and is estimated from the following equation for a spherical particle [30],

215 $$\phi = \frac{6}{\pi^2}\sum_{\mathrm{n}=1}^{\infty}\frac{1}{n^2}\exp\left(-n^2\frac{\pi^2}{r^2}D_{eff}t\right) \tag{11}$$

216 With a long drying time, Eq. (11) is simplified as,

217 $$\phi = \frac{6}{\pi^2}\exp\left(-\frac{\pi^2}{r^2}D_{eff}t\right) \tag{12}$$

218 By taking natural logarithm on both sides of Eq. (12), it becomes,

219 $$\ln\phi = \ln\frac{6}{\pi^2} - \left(\frac{\pi}{r}\right)^2 D_{eff}t \tag{13}$$

220 where D_{eff} is the moisture diffusivity and r is the biomass radius. Equation (13) means $\ln\phi$ is linearly
221 proportional to time t. Specifically, from the slope of the straight line between $\ln\phi$ and t, the moisture

diffusivity can be obtained. Based on the moisture diffusivity, the activation energy is determined from the Arrhenius equation [31],

$$D_{\text{eff}} = D_0 \exp\left(-\frac{E_a}{RT}\right) \tag{14}$$

where D_0 is the diffusivity coefficient at the infinite moisture content and E_a and R are the activation energy and the universal gas constant, respectively. The logarithmic form of Eq. (14) is given by,

$$\ln D_{eff} = \ln D_0 - \frac{E_a}{RT} \tag{15}$$

In order to obtain the activation energy, values of $\ln D_{eff}$ are plotted versus $1/T$. The activation energy is then determined from the slope of the straight line (E_a/R), as illustrated in Fig.2.

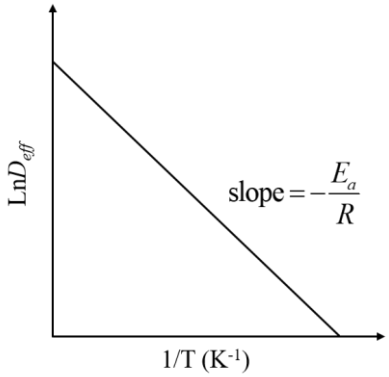

Fig. 2. Schematic plot of Eq. (15).

During the drying process in a fluidized bed biomass contacts with hot air. The temperature and interaction between solid and gas phases affect the heat and mass transfer efficiency. In order to explore the drying characteristics, the mass transfer coefficient between the gas and solid phases needs to be measured. However, due to the complexity of the fluid flow, the mass transfer coefficient is difficult to measure. In this study, the mass transfer coefficient is determined from [9],

$$k_{gp} = \frac{\dot{m}_v}{A_p \Delta\alpha_{ml}} \tag{16}$$

where k_{gp} is the mass transfer coefficient between biomass and air, $\dot{m}_v$ is the mass flow rate of water vapor transferred between biomass and air, and A_p is the surface area of biomass. Moreover, $\Delta\alpha_{ml}$ is a logarithmic mean difference in mass concentration of moisture in air, and is defined as,

$$\Delta\alpha_{ml} = \frac{\alpha_{v,s} - \alpha_{v,o}}{\ln\left(\frac{\alpha_{v,s} - \alpha_{v,i}}{\alpha_{v,s} - \alpha_{v,o}}\right)} \tag{17}$$

where $\alpha_{v,s}$, $\alpha_{v,o}$ and $\alpha_{v,i}$ represent the mass concentration of the moisture in the air on the particle surface and at the exit and entrance of the bed, respectively. The mass concentration of moisture is calculated from the ideal gas law and the moisture content. Since the equation is applied to the entire bed, then the biomass surface area is given by,

$$A_p = S_p V_p \tag{18}$$

where S_p is the particle surface area per unit particle volume and V_p is the particle volume. Furthermore, Eq. (16) is simplified as,

$$k_{gp} = \frac{\rho_{p,0}(-\eta)}{S_p \Delta\alpha_{ml}} \tag{19}$$

where $\rho_{p,0}$ is the density of dry biomass. In summary, based on the real-time measurement of the moisture content distribution using the electrostatic sensor array, the mass transfer coefficient distribution between the gas and solid phases can be measured from Eq. (19).

2.4. Experimental conditions

2.4.1 Experimental setup

In order to investigate the drying kinetics of biomass using the proposed method, experimental tests were carried out on an experimental fluidized bed dryer. In view of the advantages in system installation and result visualization, a pseudo two-dimensional (2D) bed with a relatively small thickness was deployed in this study. It is known that flow patterns in a 3D bed are different from those in a 2D bed. Therefore, the translation of results obtained for a 2D bed to 3D bed or industrial systems has to be done with caution. However, research on 2D fluidized beds is still valuable for the calibration of measurement systems and the validation of numerical models [32]. Fig. 3 shows the overview of the fluidized bed and the installation of the measurement system. The fluidized bed is made of plexiglass with a height of 850 mm, a width of 150 mm and a thickness of 30 mm. Since the thickness of the bed is much smaller than its height and width, the bed can be regarded as a pseudo 2D fluidized bed with the movement of fluid in the thickness direction being ignored. The entire electrostatic sensing unit used was constructed in-house [21]. The electrostatic sensor array, mounted on back of the fluidized bed (100 mm above the distributor), is composed of multiple

electrodes for measuring the drying kinetics of biomass. To cover the main section of the fluidized bed, the overall dimension of the sensor array board is 150 mm × 64 mm. The electrodes were manufactured on a printed circuit board with a thickness of 1 mm. Each electrode is 10 mm in length and 3 mm in width. The center-to-center spacing between a pair of adjacent electrodes is 16 mm. Furthermore, the digital imaging unit consists of an illumination source as well as a digital camera (Fastcam Mini UX50) with a resolution of 1280 × 1024 pixels and a frame rate up to 500 frames per second. The imaging unit was placed on the front of the bed, which allows to visualize the primary drying zone of the bed. To enhance the contrast of images, a black background was deployed at the back of the bed, as shown in Fig. 3. During the drying experiments the electrostatic sensing and digital imaging units collected data (sensor signals and images) simultaneously. A multiple-channel signal conditioning unit and a NI USB-6363 DAQ were utilized to acquire the signals from the electrostatic sensing unit with a sampling frequency of 1 kHz. To study the drying kinetics under different operating conditions, biomass particles were dried at five air velocities and five air temperatures, as summarized in Table 1. The air flow rate was metered and controlled using a rotameter and a needle valve. The fluidized bed is also equipped with a PID-adjusted temperature controller and an air preheater to ensure the stabilization of the air temperature. The relative humidity of the air entering the fluidized bed was set to constant at 7% during the tests.

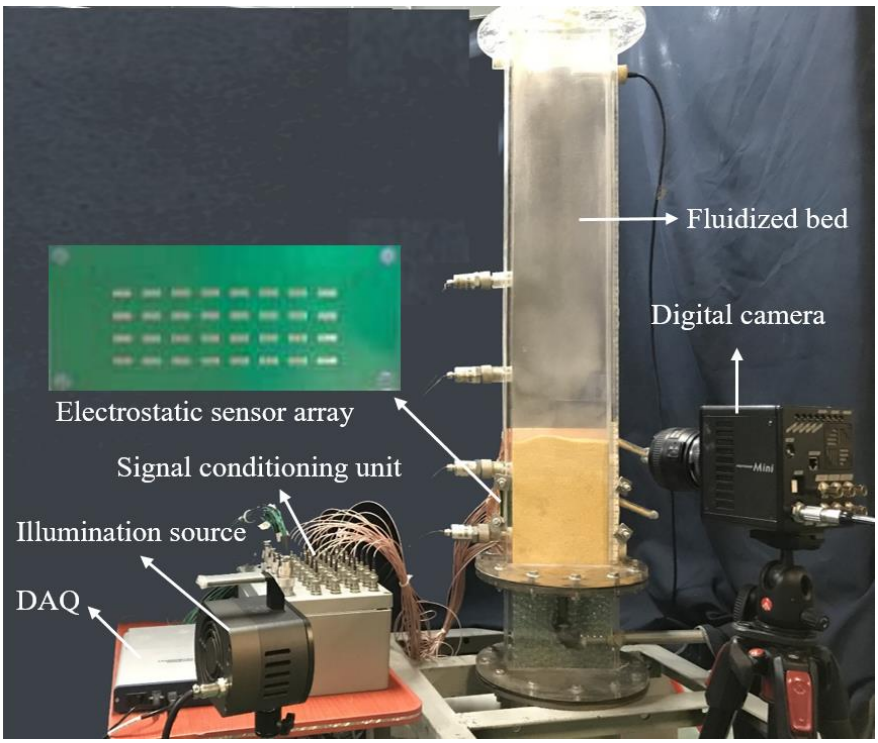

Fig. 3. Experimental setup.

Table 1 Experimental conditions

Air temperature T (℃)	Air velocity V (m/s)				
	0.31	**0.37**	**0.43**	**0.49**	**0.56**
45	T1V1	T1V2	T1V3	T1V4	T1V5
52	T2V1	T2V2	T2V3	T2V4	T2V5
60	T3V1	T3V2	T3V3	T3V4	T3V5
67	T4V1	T4V2	T4V3	T4V4	T4V5
75	T5V1	T5V2	T5V3	T5V4	T5V5

2.4.2 Test material

Corn is a typical biomass material and utilized as a renewable fuel in some thermal power plants [33]. In this study corn kernels after grinding were used as test particles. The bulk density and mean diameter of corn kernels are about 1100 kg/m^3 and 1 mm, respectively. Such physical properties mean corn kernels are regarded as Geldart D particles [34]. The initial moisture content of corn kernels is 16.5 wt.%, which was measured with the Halogen Moisture Analyzer. All corn kernels were stored in an environmental chamber (LY-2225, Liyi Dongguan) with constant temperature and humidity for at least 6 hours to ensure uniform moisture distribution across the particles before testing. The minimum fluidization velocity for corn kernels is approximately 0.216 m/s, which was experimentally determined using a conventional differential pressure method [21].

3. Experimental results and discussion

3.1. Moisture content

A typical example of moisture contents obtained from the electrostatic sensing method under the operating condition of T3V3 is shown in Fig. 4. To elucidate the discrepancies in the drying kinetics of biomass at different locations, the drying curves of biomass at the interior, boundary and exterior of the bubble are plotted in Fig. 4. The standard deviation, given in the form of error bars in Fig. 4, indicates the range of fluctuations in the measured moisture content under each test condition. The standard deviation at each data point is determined from the repeated measurements of moisture content over a total duration of 20 s.

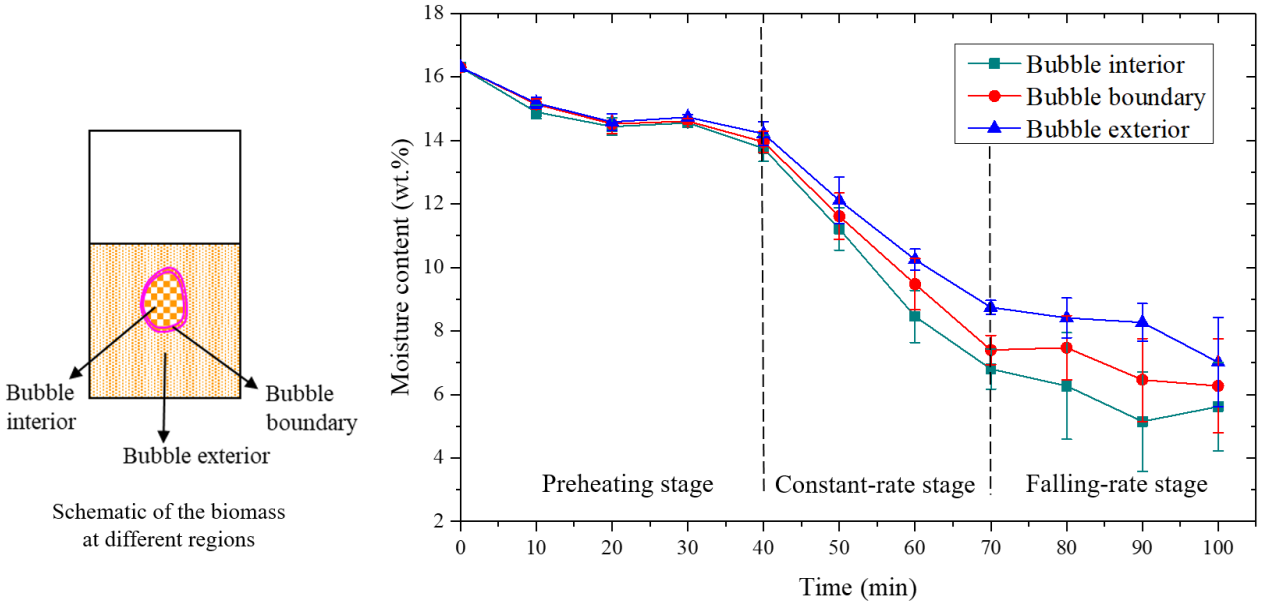

Fig. 4. Measured moisture content. (a) Definitions of different regions of the bubble in a bed. (b) Drying curves of biomass at different locations under the condition of T3V3.

The time histories of moisture content during the drying process are divided into three stages, namely preheating stage, constant-rate stage and falling-rate stage, respectively [14]. In the preheating stage, channeling and agglomeration occur and biomass particles are not fluidized due to high moisture. No obvious discrepancy in the moisture content in biomass at different locations is observed. The moisture content in biomass reduces gradually as the drying process progresses. The particles are dried with the movement of bubbles and the flow behaviors become turbulent [25]. Besides, the moisture content in biomass in the bubble is lower than that at the boundary and exterior of the bubble during the constant-rate stage. This can be explained that there is more effective contact between biomass particles in the bubble and hot air. As shown in Fig. 4, the measured moisture content at different locations generally yields a more significant discrepancy in the falling-rate stage. Since the flow becomes more turbulent and large bubbles are generated in the later period of the drying, which facilitates the convective mass transfer between the gas and solid phases.

3.2. Drying models

As described in Section 2, the measured moisture content in biomass is converted into moisture ratio for the comparison of the drying models. The data are fitted with the five models (Section 2.3), as shown in Fig. 5.

Moreover, the goodness of fit is evaluated through the determination coefficient (R^2) and the reduced Chi square (χ^2) [35],

$$R^2 = 1 - \left(\frac{\sum_{i=1}^{N} \left(\phi_{\exp,i} - \phi_{\mathrm{pre},i} \right)^2}{\sum_{i=1}^{N} \left(\phi_{\exp,mean} - \phi_{\mathrm{pre},i} \right)^2} \right) \tag{20}$$

$$\chi^2 = \frac{1}{N\text{-}P} \left[\sum_{i=1}^{N} \left(\phi_{\exp,i} - \phi_{\mathrm{pre},i} \right)^2 \right] \tag{21}$$

where $\phi_{exp,mean}$ is the mean moisture ratio from the experimental results and P is the number of parameters in the fitting function. The list of calculated parameters in the model equations (Eqs. (5) − (9)) for particles at different locations and their evaluation criteria are summarized in Table 2. The higher the R^2 value and the lower the χ^2 value, the better the goodness of fit.

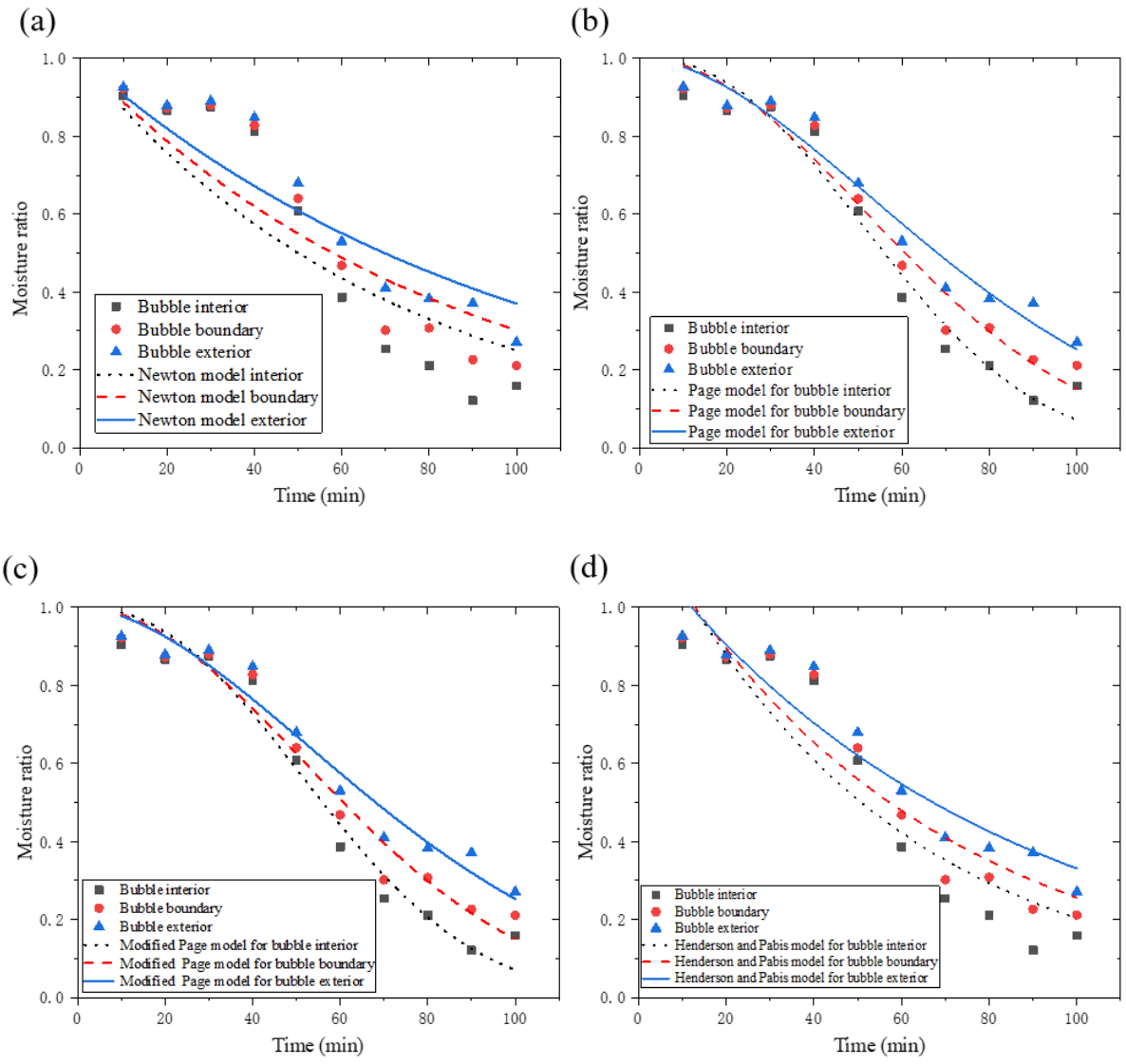

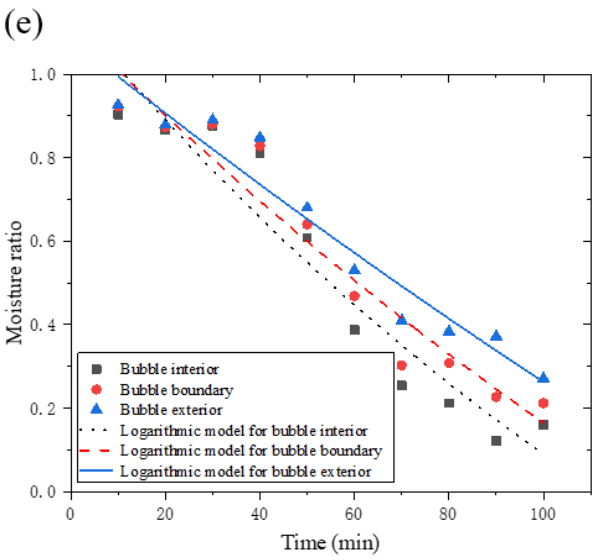

Fig. 5. Fitted curves of various drying models under T3V3 operating condition. (a) Newton model. (b) Page model. (c) Modified Page model. (b) Henderson and Pabis model. (e) Logarithmic model.

Table 2 Model parameters and evaluation criteria (T3V3)

Model		Parameters			Evaluation criteria	
		k	***n* or *a***	***c***	R^2	χ^2
Newton	**Interior**	0.01385	—	—	0.79267	0.02165
	Boundary	0.01196	—	—	0.82384	0.01529
	Exterior	0.00956	—	—	0.85185	0.00956
Page	**Interior**	0.00006	2.30674	—	0.96357	0.00437
	Boundary	0.00018	2.01153	—	0.96173	0.00374
	Exterior	0.00363	1.78962	—	0.95875	0.00299
Modified page	**Interior**	0.01524	2.30674	—	0.95902	0.00455
	Boundary	0.01374	2.01163	—	0.95695	0.00394
	Exterior	0.01195	1.78156	—	0.9536	0.00309
Henderson and Pabis	**Interior**	0.01825	1.2633	—	0.84828	0.01616
	Boundary	0.01562	1.22267	—	0.87611	0.01075
	Exterior	0.01258	1.16391	—	0.90596	0.00682
Logarithmic	**Interior**	0.00538	2.54995	-1.4	0.91271	0.0093
	Boundary	0.00366	3.12087	-2	0.92593	0.00643
	Exterior	0.00197	4.58356	-3.5	0.94081	0.00429

It has been observed from the R^2 and χ^2 values that the Page model shows the best fit with the experimental data. In other words, the Page model is most suitable for the drying process of biomass under the given conditions.

3.3. Moisture diffusivity

Moisture diffusivity is useful for describing the moisture transfer rate in biomass. In addition, previous research highlighted the air temperature has an effect on the moisture diffusivity [18]. Therefore, the experimental results at an air velocity of 0.43 m/s for five air temperatures from 45 ℃ to 75 ℃ (i.e. T1V3 − T5V3) are analyzed. As indicated by Eq. (13), the moisture diffusivity values of biomass under different conditions are calculated using the method described in Section 2.3. Fig. 6 shows the results under the operating conditions of T1V3 − T5V3.

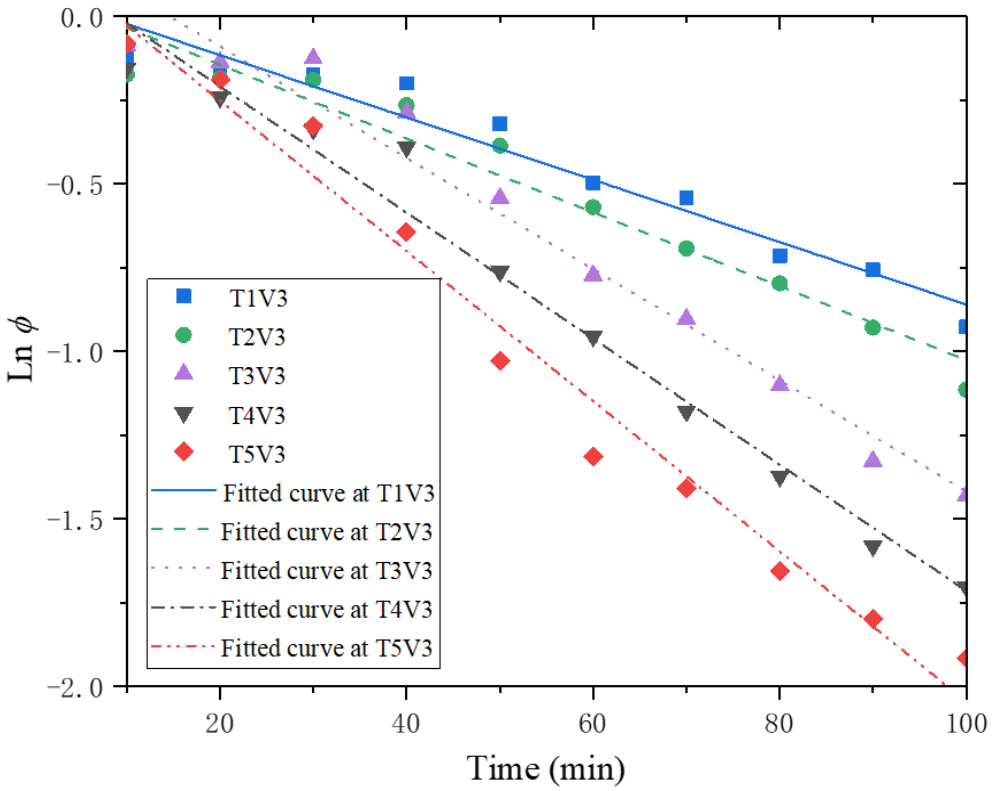

Fig. 6. Fitted curves of biomass under different drying conditions.

From Fig. 6, it can be observed that, for a given condition, the moisture diffusivity of biomass increases with air temperature. The moisture diffusivity values are 9.43×10^{-10}, 1.12×10^{-9}, 1.68×10^{-9}, 1.91×10^{-9} and 2.27×10^{-9} m^2/s, respectively, under the operating conditions of T1V3−T5V3. The results indicate that temperature is an important factor affecting the moisture diffusivity, which is consistent with previous studies [18, 36]. In order to gain further insight of the moisture diffusivity of biomass at different locations, the moisture diffusivity results obtained under all test conditions are listed in Table 3.

Table 3 Moisture diffusivity values under different drying conditions.

Drying condition		D_{eff} (m^2/s)	R^2
T1V3	**Interior**	7.69×10^{-10}	0.96
	Boundary	7.58×10^{-10}	0.87
	Exterior	7.10×10^{-10}	0.96
T2V3	**Interior**	8.42×10^{-10}	0.92
	Boundary	7.98×10^{-10}	0.90
	Exterior	7.71×10^{-10}	0.90
T3V3	**Interior**	2.26×10^{-9}	0.89
	Boundary	1.85×10^{-9}	0.90
	Exterior	1.66×10^{-9}	0.93
T4V3	**Interior**	2.44×10^{-9}	0.93
	Boundary	1.90×10^{-9}	0.89
	Exterior	1.73×10^{-9}	0.95
T5V3	**Interior**	2.48×10^{-9}	0.89
	Boundary	1.92×10^{-9}	0.89
	Exterior	1.76×10^{-9}	0.87

Table 3 show that the moisture diffusivity of biomass at the interior of the bubble is slightly higher than that at the boundary and exterior of the bubble under different drying conditions. A high diffusivity of biomass in the bubble is caused by its good contact with hot air, which facilitates the moisture transfer.

In general, the activation energy E_a presents the energy barrier that is required to overcome during diffusion of the water molecules through the particles [31]. From the moisture diffusivity at an air velocity of 0.43 m/s (V3), a graph between ln(D_{eff}) and 1/T is plotted in Fig. 7.

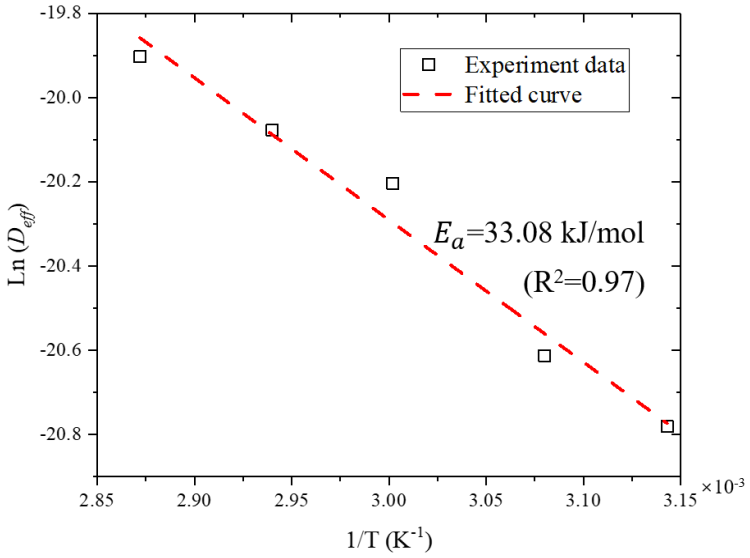

Fig. 7. Activation energy of biomass under the condition of V3.

As shown in Fig. 7, a good linear relationship exists between ln(D_{eff}) and 1/T. Moreover, the activation energies of biomass at different locations are compared. The activation energies of biomass at the interior, boundary and exterior of the bubble calculated from Eq. (14) are 42.07, 33.15 and 32.73 kJ/mol, respectively. It is found from the results that the activation energy under a given condition decreases in the order of the interior, boundary and exterior of the bubble. According to the Fick's law, the moisture diffusion is a function of moisture gradient. A greater moisture gradient is produced when particles in the bubble contact more efficiently with the hot air, thus leading to a higher energy required for water diffusion [36].

3.4. Mass transfer coefficient

The gas-solid mass transfer coefficient is an important parameter in the drying kinetics. In this paper, the mass transfer coefficient is obtained using the method described in Section 2. Fig. 8 illustrates the results of the average mass transfer and mass transfer coefficient distribution.

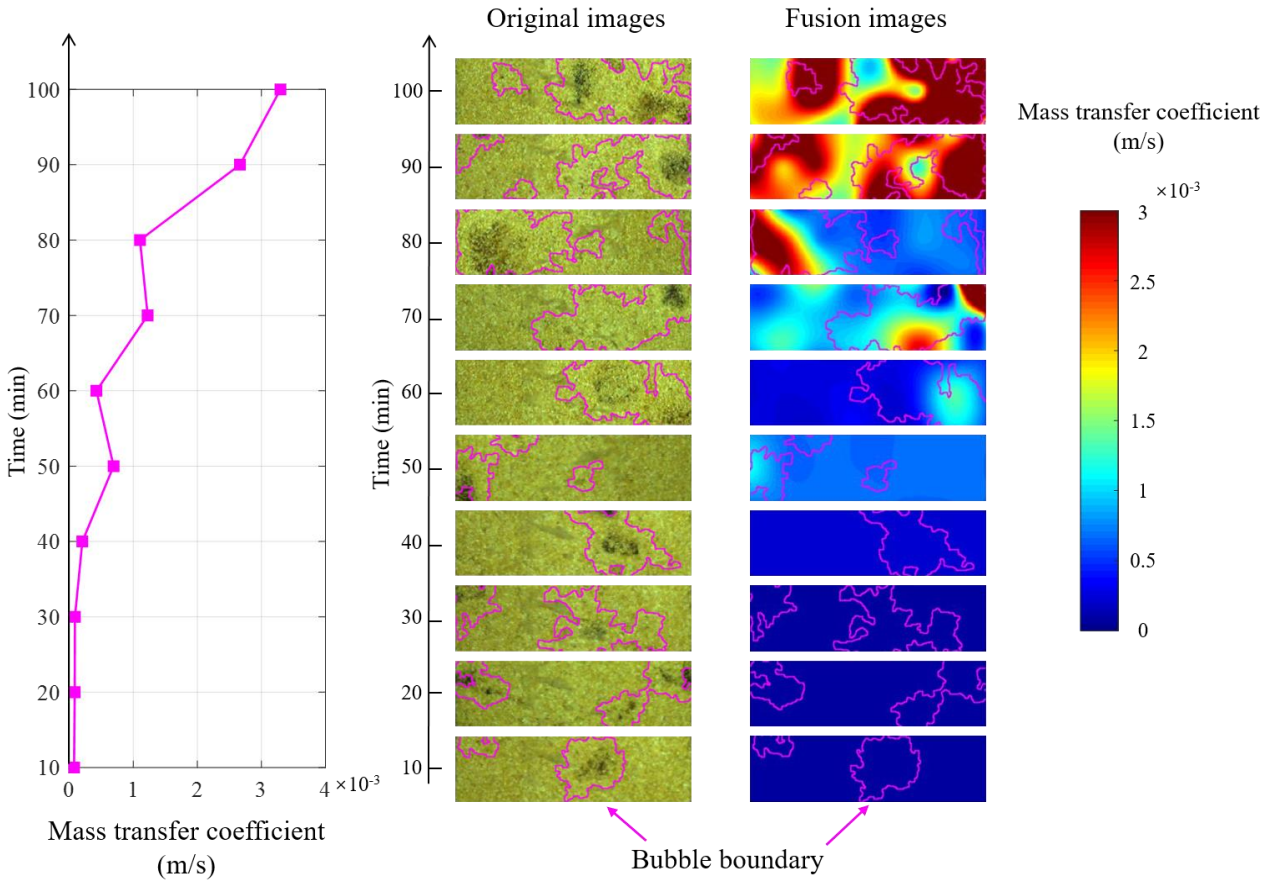

Fig. 8. Average mass transfer coefficient and mass transfer coefficient distribution (T3V3).

The average mass transfer coefficient is determined by averaging the mass transfer coefficients at all pixels of the fusion images whilst the mass transfer coefficient distribution is obtained using the mass transfer

coefficient at each pixel and the BSI algorithm. The bubble boundaries are marked with pink lines on the original images and fusion images. The average mass transfer coefficient of biomass, increasing significantly from 7×10^{-5} m/s to 3.4×10^{-3} m/s as shown in Fig. 8, is determined from the experimental results of the drying process under the condition of T3V3. Moreover, the mass transfer coefficients of biomass at different locations along with the corresponding standard deviations are also calculated (Fig. 9).

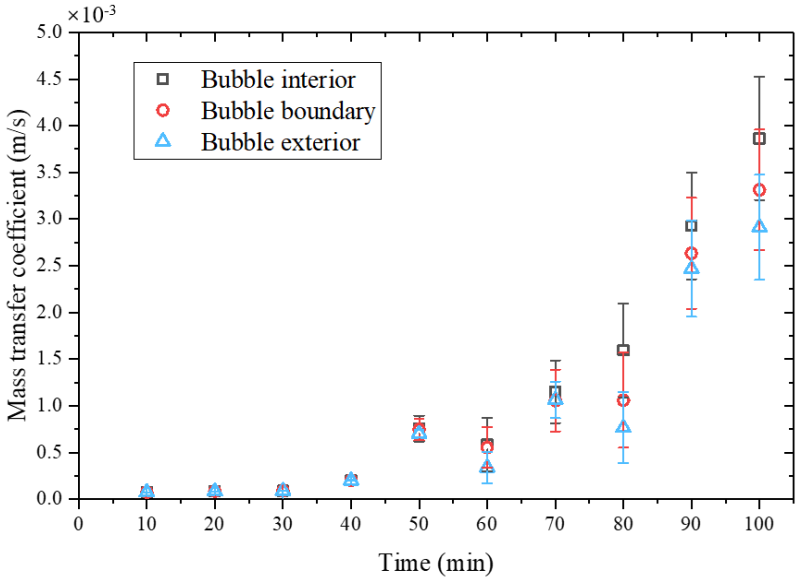

Fig. 9. Mass transfer coefficients of biomass at different locations (T3V3).

It is evident that the mass transfer coefficients of particles at different locations are almost the same during the preheating stage, while the coefficients increase to different values during the falling-rate stage. Compared to the gas-solid mass transfer coefficients at different locations, the mass transfer coefficient in the bubble is slightly higher than that at the boundary and exterior of the bubble. The main reason for this is that, during the later stage of the drying, the channeling and biomass agglomeration phenomena disappear in the bed. The high temperature of the bubble enhances the migration rate of the water molecules between the gas and solid phases. Meanwhile, the bubble with low moisture content causes the large moisture gradient between the gas and solid phases, resulting in the great mass transfer.

To investigate the effects of the air temperature and air velocity on the mass transfer of biomass in the bed, the average mass transfer coefficients of biomass under various conditions along with the corresponding standard deviation are calculated, as illustrated in Fig. 10.

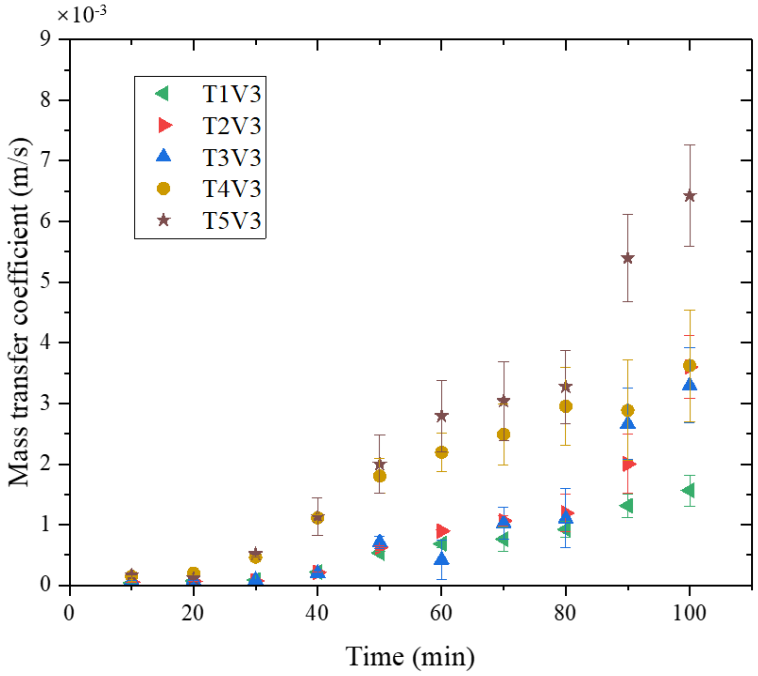

(a) Results at various air temperatures and a given air velocity.

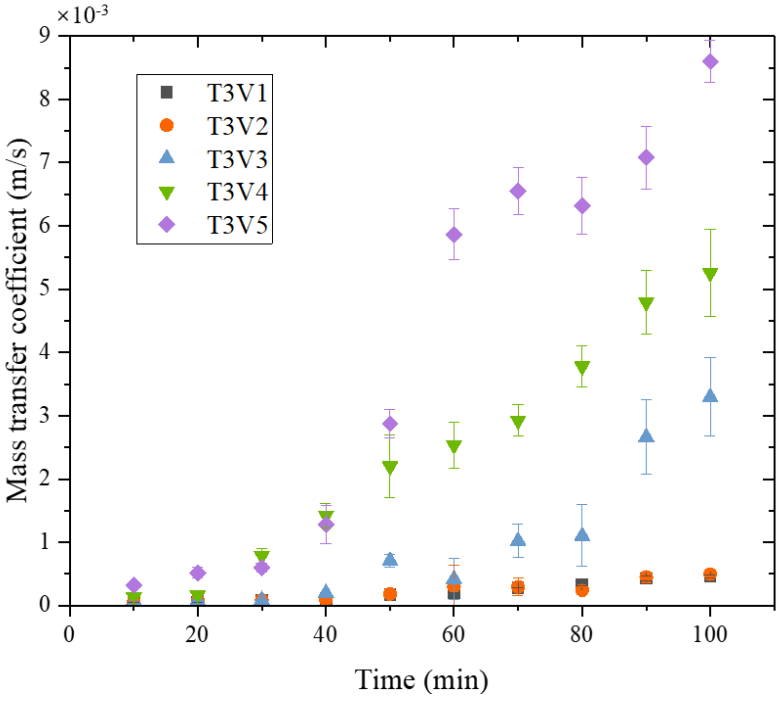

(b) Results at various air velocities and a given air temperature.

Fig. 10. Gas-solid mass transfer coefficients under various operating conditions.

As shown in Fig. 10, the average mass transfer coefficients rise to 6.43×10^{-3} m/s and 8.61×10^{-3} m/s at 100 min under T5V3 and T3V5 operating conditions, respectively. Fig.11 depicts the gas-sloid mass transfer coefficients at 100 min under all operating conditions.

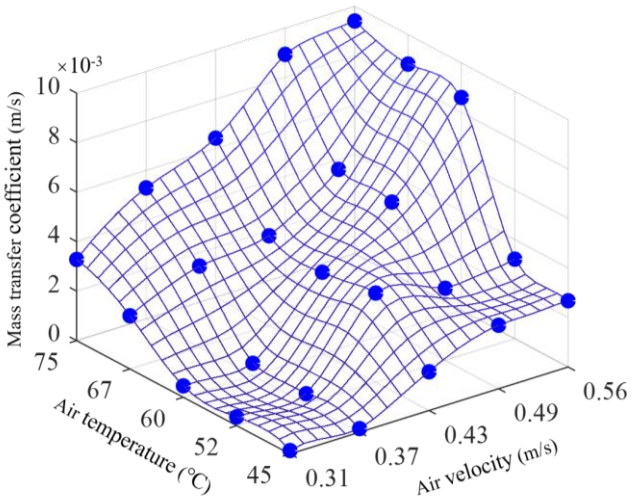

Fig. 11. Gas-solid mass transfer coefficients at 100 min under all operating conditions.

Fig. 11 indicates that, for a given condition, gas-solid mass transfer coefficient increases significantly with air temperature and air velocity. Similar results about the effects of the air temperature and air velocity on the mass transfer coefficient were found by Huang *et al.* [37]. In general, a higher air temperature results in moisture migration more easily. Besides, as implied by the thin layer model [13], increasing the hot air velocity leads to reduced boundary layer of the convective heat and mass transfers between the gas and solid phases, and also gives rise to moisture moving away from biomass surface. Meanwhile, water evaporation rates grow up both with the air temperature and with the air velocity, thus the discrepancy in moisture content between internal and surface water in biomass tends to increase, indicating an enhanced mass transfer occurs.

It is seen from the experimental results under all operating conditions that higher gas-solid heat and mass transfers in the dryer are produced at a higher air temperature or air velocity, resulting in greater drying efficiency. However, it should be emphasized that the drying efficiency may not always be the optimal at a high air temperature and a high air velocity. This is because the quality of biomass needs to be considered under the high air temperature condition. The high temperature may overheat biomass, which may cause serious damage to its quality such as color, porosity, and the bioactive compound content [9]. Moreover, a high air velocity may bring up the slugs and the flow pattern in the bed change into a slug flow, which is harmful for the drying reaction. Fig. 12 shows the slug flow formed in the fluidized bed under the condition of T5V5 (i.e. air velocity of 0.56 m/s and air temperature of 75 ℃). The high air velocity and air temperature facilitate the merging of bubbles and formation of a slug. The size of the slug is close to the width of the bed,

which inhibits the fluidization and drying. While under other drying conditions, the flow pattern in the fluidized bed is almost bubbling flow, and no slug flow pattern is found.

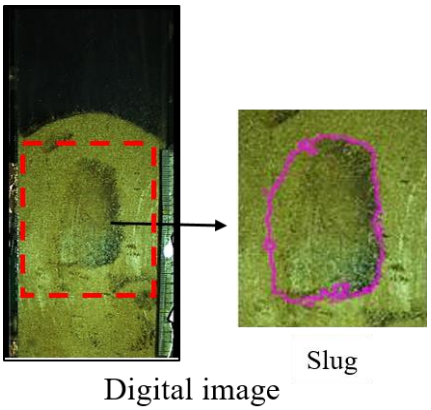

Fig. 12. Slugging flow pattern (T5V5).

4. Conclusions

The drying kinetics of biomass in a fluidized bed dryer have been experimentally studied using the electrostatic sensing and digital imaging techniques under a range of air temperatures from 45 ℃ to 75 ℃ at an air velocity from 0.31 m/s to 0.56 m/s. In this work, the moisture content distribution of biomass and bubble distribution in the fluidized bed have been obtained from the signals from the electrostatic sensor array and original images from the digital camera, respectively. By fusing the above results, the drying kineties of biomass at the interior, boundary and exterior of the bubble are obtained using the proposed method, which helps to analyze and improve the drying model at different regions. The experimental results have shown that the Page model is most suitable for describing the decline of the moisture content in biomass at different locations in the bed. Biomass in the bubble has a higher moisture diffusivity, which is related to the higher temperature of the hot air in the bubble. It is found from the results at an air temperature from 45 ℃ to 75 ℃ that the activation energy of biomass in the bubble increases slightly in comparison to that at the boundary and exterior of the bubble, indicating the divergence in the drying characteristics at different locations.

In addition, compared with the gas-solid mass transfer coefficients of biomass at the boundary and exterior of the bubble, the mass transfer coefficient of biomass in the bubble is larger, which is attributed to the efficient contacts between the biomass particles and the hot air. Furthermore, it is observed from the experimental results that the gas-solid mass transfer depends on the air temperature and air velocity, while the highest air temperature and the highest air velocity may not be the optimal drying condition. It is

envisaged that an industrial measurement system based on the proposed methodology will be constructed and evaluated on a large-scale fluidized bed dryer in the near future.

Acknowledgement

This work was supported by the National Natural Science Foundation of China (No. 61403138) and Beijing Natural Science Foundation (No. 3202028).

References

[1] Shi Y, Liu QW, Shao YJ, Zhong WQ. Energy and exergy analysis of oxy-fuel combustion based on circulating fluidized bed power plant firing coal, lignite and biomass. Fuel 2020;269:117424.

[2] Kuba M, Skoglund N, Ohman M, Hofbauer H. A review on bed material particle layer formation and its positive influence on the performance of thermo-chemical biomass conversion in fluidized beds. Fuel 2021;291:120214.

[3] Motta IL, Miranda NT, Filho RM, Maciel MRW. Biomass gasification in fluidized beds: a review of biomass moisture content and operating pressure effects. Renew Sust Energ Rev 2018;94:998–1023.

[4] Verma M, Loha C, Sinha AN, Chatterjee PK. Drying of biomass for utilising in cofiring with coal and its impact on environment – a review. Renew Sust Energ Rev 2017;71:732–741.

[5] Gumienna M, Szwengiel A, Lasik M, Szambelan K, Majchrzycki D, Adamczyk J, Nowak J, Czarnecki Z. Effect of corn grain variety on the bioethanol production efficiency. Fuel 2016;164:386–392.

[6] Kaplan O, Celik C. An experimental research on woodchip drying using a screw conveyor dryer. Fuel 2018;215:468–473.

[7] Paczkowski S, Labbé R, Sauer C, Anetzberger A, Russ M, Wöhler M, Jaeger D, Pelz S. A novel approach to improve the energy and cost efficiency of feedstock drying for pellet production. Fuel 2021;290:119805.

[8] Yogendrasasidhar D, Setty YP. Drying kinetics, exergy and energy analyses of Kodo millet grains and Fenugreek seeds using wall heated fluidized bed dryer. Energy 2018;151:799–811.

[9] Sozzi A, Zambon M, Mazza G, Salvatori D. Fluidized bed drying of blackberry wastes: drying kinetics, particle characterization and nutritional value of the obtained granular solids. Powder Technol 2021;385:37–49.

[10] Moreno RM, Antolin G, Reyes AE. Mass transfer during forest biomass particles drying in a fluidised bed. Biosyst Eng 2020;198:163–171.

[11] Aghbashlo M, Sotudeh-Gharebagh R, Zarghami R, Mujumdar AS, Mostoufi N. Measurement techniques to monitor and control fluidization quality in fluidized bed dryers: a review. Dry Technol 2014;32:1005–1051.

[12] Kucuk H, Midilli A, Kilic A, Dincer I. A review on thin-layer drying-curve equations. Dry Technol 2014;32:757–773.

[13] Chen DY, Zheng Y, Zhu XF. In-depth investigation on the pyrolysis kinetics of raw biomass. Part I: Kinetic analysis for the drying and devolatilization stages. Bioresour Technol 2013;131:40–46.

[14] Zeng X, Wang F, Adamu MH, Zhang LJ, Han ZN, Xu GW. High-temperature drying behavior and kinetics of lignite tested by the micro fluidization analytical method. Fuel 2019;253:180–188.

[15] Ge LC, Liu XY, Feng HC, Jiang H, Chu HQ, Xu C, Wang ZH. Enhancement of lignite microwave dehydration by cationic additives. Fuel 2021;289:119985.

[16] Chen GB, Maier DE, Campanella OH, Takhar PS. Modeling of moisture diffusivities for components of yellow-dent corn kernels. J Cereal Sci 2009;50:82–90.

[17] Jia DN, Bi XT, Lim CJ, Sokhansanj S, Tsutsumi A. Gas-solid mixing and mass transfer in a tapered fluidized bed of biomass with pulsed gas flow. Powder Technol 2017;316:373–387.

[18] Koukouch A, Idlimam A, Asbik M, Sarh B, Izrar B, Bostyn S, Bah A, Ansari O, Zegaoui O, Amine A. Experimental determination of the effective moisture diffusivity and activation energy during convective solar drying of olive pomace waste. Renew Energ 2017;101:565–574.

[19] Medrano JA, Gallucci F, Boccia F, Alfano N, Van Sint Annaland M. Determination of the bubble-to-emulsion phase mass transfer coefficient in gas-solid fluidized beds using a non-invasive infra-red technique. Chem Eng J 2017;325:404–414.

[20] Jia D, Bi XT, Lim CJ, Sokhansanj S, Tsutsumi A. Biomass drying in a pulsed fluidized bed without inert bed particles. Fuel 2016;186:270–284.

[21] Qi BJ, Yan Y, Zhang WB, Wang XY. Measurement of biomass moisture content distribution in a fluidised bed dryer through electrostatic sensing and digital imaging. Powder Technol 2021;388:380–392.

[22] Wang HG, Yang WQ. Application of electrical capacitance tomography in pharmaceutical fluidised beds – a review. Chem Eng Sci 2021;231: 116236.

[23] Rimpilainen V, Heikkinen LM, Vauhkonen M. Moisture distribution and hydrodynamics of wet granules during fluidized-bed drying characterized with volumetric electrical capacitance tomography. Chem Eng Sci 2012;75: 220–234.

[24] Zhang WB, Cheng XF, Hu YH, Yan Y. Online prediction of biomass moisture content in a fluidized bed dryer using electrostatic sensor arrays and the Random Forest method. Fuel 2019;239:437– 445.

[25] Zhang WB, Cheng XF, Hu YH, Yan Y. Measurement of moisture content in a fluidized bed dryer using an electrostatic sensor array. Powder Technol 2018;325:49–57.

[26] Qi BJ, Yan Y, Zhang WB, Li XY. Experimental investigations into bubble characteristics in a fluidized bed through electrostatic imaging. IEEE Trans Instrum Meas 2021;70: 9503813.

[27] Gáspár C. Multigrid technique for biharmonic interpolation with application to dual and multiple reciprocity method. Numer Algorithms 1999;21:165–183.

[28] Wei S, Wang ZH, Wang FH, Xie WJ, Chen PX, Yang DY. Simulation and experimental studies of heat and mass transfer in corn kernel during hot air drying. Food Bioprod Process 2019;117:360–372.

[29] Meziane S. Drying kinetics of olive pomace in a fluidized bed dryer. Energy Convers Manage 2011;52:1644–1649.

[30] Khanali M, Banisharif A, Rafiee S. Modeling of moisture diffusivity, activation energy and energy consumption in fluidized bed drying of rough rice. Heat Mass Transf 2016;52:2541–2549.

[31] Adamu MH, Zeng X, Zhang JL, Wang F, Xu GW. Property of drying, pyrolysis, gasification, and combustion tested by a micro fluidized bed reaction analyzer for adapting to the biomass two-stage gasification process. Fuel 2020;264:116827.

[32] Ma JL, Liu DY, Chen XP. Bubbling behavior of cohesive particles in a two-dimensional fluidized bed with immersed tubes. Particuology 2017;31:152–160.

[33] López R, Fernández C, Cara J, Martínez O, Sánchez ME. Differences between combustion and oxy-combustion of corn and corn–rape blend using thermogravimetric analysis. Fuel Process Technol 2014;128:376–387.

[34] Geldart D. Types of gas fluidization. Powder Technol 1973;7:285–292.

[35] Kaleta A, Górnicki K, Winiczenko R, Chojnacka A. Evaluation of drying models of apple (var. Ligol) dried in a fluidized bed dryer. Energy Convers Manage 2013;67:179–185.

[36] Gómez-de la Cruz FJ, Palomar-Carnicero JM, Hernandez-Escobedo Q, Cruz-Peragon F. Determination of the drying rate and effective diffusivity coefficients during convective drying of two-phase olive mill waste at rotary dryers drying conditions for their application. Renew Energ 2020;153:900–910.

[37] Huang YW, Chen MQ, Jia L. Assessment on thermal behavior of municipal sewage sludge thin-layer during hot air forced convective drying. Appl Therm Eng 2016;96:209–216.